Nasal chitosan microparticles target a zidovudine prodrug to brain HIV sanctuaries

# Nasal chitosan microparticles target a zidovudine prodrug to brain HIV sanctuaries

Alessandro Dalpiaz [a], Marco Fogagnolo [a], Luca Ferraro [b], Antonio Capuzzo [b], Barbara Pavan [b], Giovanna Rassu [c,*], Andrea Salis [c], Paolo Giunchedi [c], Elisabetta Gavini [c]

[a] *Department of Chemical and Pharmaceutical Sciences, University of Ferrara, via Fossato di Mortara 19, 44121 Ferrara, Italy*

[b] *Department of Life Sciences and Biotechnology, University of Ferrara, via Borsari 46, 44121 Ferrara, Italy*

[c] *Department of Chemistry and Pharmacy, University of Sassari, via Muroni 23/a, 07100 Sassari, Italy*

*E-mail addresses*: dla@unife.it (A. Dalpiaz), marco.fogagnolo@unife.it (M. Fogagnolo), frl@unife.it (L. Ferraro), antonio.capuzzo@unife.it (A. Capuzzo), pvnbbr@unife.it (B. Pavan), grassu@uniss.it (G. Rassu), asalis@uniss.it (A. Salis), pgiunc@uniss.it (P. Giunchedi), eligav@uniss.it (E. Gavini).

* Corresponding author: Giovanna Rassu, Department of Chemistry and Pharmacy, University of Sassari, via Muroni 23/a, 07100 Sassari, Italy. Tel: +39 079228735; Fax: +39 079228733; E-mail address: grassu@uniss.it

## ABSTRACT

Zidovudine (AZT) is an antiretroviral drug that is a substrate of active efflux transporters (AETs) that extrude the drug from the central nervous system (CNS) and macrophages, which are considered to be sanctuaries of HIV. The conjugation of AZT to ursodeoxycholic acid is known to produce a prodrug (UDCA-AZT) that is able to elude the AET systems, indicating the potential ability of this prodrug to act as a carrier of AZT in the CNS and in macrophages. Here, we demonstrate that UDCA-AZT is able to permeate and remain in murine macrophages with an efficiency twenty times higher than that of AZT. Moreover, we propose the nasal administration of this prodrug in order to induce its uptake into the CNS. Chitosan chloride-based microparticles (CP) were prepared by spray-drying and were characterized with respect to size, morphology, density, water uptake and the dissolution profile of UDCA-AZT. The CP sample was then nasally administered to rats. All *in vitro* and *in vivo* measurements were also performed for a CP parent physical mixture. The CP sample was able to increase the dissolution rate of UDCA-AZT and to reduce water uptake with respect to its parent physical mixture, inducing better uptake of UDCA-AZT into the cerebrospinal fluid of rats, where the prodrug can act as an AZT carrier in macrophages.



*Keywords:* Zidovudine prodrug, HIV treatment, macrophage, brain targeting, nasal formulation, chitosan microparticle


*Chemical compounds studied in this article:*

Zidovudine (PubChem CID: 35370); Chitosan (PubChem CID: 21896651)

## 1. Introduction

Combination antiretroviral therapy (cART) has made a significant impact against HIV infection. However, the efficacy of this therapy is limited by the poor bioavailability of anti-HIV drugs at viral reservoir sites, such as the central nervous system (CNS) (Cunningham et al., 2000; Kolson and Gonzalez-Scarano, 2000), particularly in cerebrospinal fluid (CSF) subarachnoid spaces that contain macrophages, which constitute the only site of HIV replication in the brain (Cunningham et al., 1997; Ghersi-Egea et al., 1996). The lack of drug penetration into these "HIV sanctuaries" occurs primarily due to the expression of active efflux transporters (AETs) on the blood−brain (BBB) and blood−cerebrospinal fluid (BCSFB) barriers (Namanja et al., 2012; Pavan and Dalpiaz, 2011). *In vivo,* these transporters induce the asymmetric transport of anti-HIV drugs across these barriers, where the rate of drug efflux from the CNS to the blood is greater than the influx rate (Wang and Sawchuk, 1995).

We recently proved that the conjugation of zidovudine (AZT), which is an antiretroviral drug used in cART protocols (De Clercq, 2009), with the bile acid ursodeoxycholic acid (UDCA) generates a prodrug (UDCA−AZT) that can elude the AET systems (Dalpiaz et al., 2012). We have therefore proposed that when this prodrug is taken up in the CNS, it should not be extruded into the bloodstream because it is able to elude the AET systems. Accordingly, we demonstrated that the nasal administration of solid lipid microparticles loaded with the UDCA-AZT prodrug facilitates its uptake into the CSF of rats (Dalpiaz et al., 2014). Nasal administration constitutes a potentially efficacious way of achieving the brain uptake of neuroactive agents (Fine et al, 2014, 2015; Illum, 2000; Vyas et al., 2005). Indeed, drugs deposited on the olfactory epithelium of the nose can gain direct access to the CNS, particularly the CSF, via transcellular transport through olfactory epithelial cells. The drugs absorbed in the CSF can then diffuse into the interstitial fluid (ISF) and subsequently penetrate the brain parenchyma (Illum, 2000, 2004; Thorne and Frey, 2001). Moreover, drugs

deposited on the olfactory epithelium can be transported into the brain parenchyma by olfactory neurons or trigeminal nerves that reach the nasal cavity (Finger et al., 1990; Illum, 2000; Johnson et al., 2010). Finally, nasally administered drugs can be absorbed into the systemic circulation from the respiratory epithelium (Cho et al, 2014) and can then reach the CNS if they are able to cross the BBB (Illum, 2000).

In general, appropriate strategies are required to improve the brain delivery of drugs, such as the addition of penetration enhancers and mucoadhesive materials to formulations or the preparation of micro- and nano-particulate delivery systems (Casettari and Illum, 2014; Dalpiaz et al., 2008; Horvát et al., 2009; Mistry et al., 2009; Rassu et al., 2015a). In this regard, chitosan is a polysaccharide derived from the alkaline deacetylation of chitin that is used in different formulations for the nose-to-brain delivery of drugs (Casettari and Illum, 2014) due to its biocompatibility, nontoxicity and high charge density, which confers mucoadhesive properties (Bernkop-Schnürch and Dünnhaupt, 2012; Sinha et al, 2004). Chitosan is poorly soluble in water at physiologic pH values, but it forms salts with inorganic or organic acids, such as hydrochloride and glutamic acid, that are soluble in water and possess better characteristics than chitosan itself, such as mucoadhesiveness and the ability to enhance the penetration of neuroactive agents into the CNS (Dalpiaz et al., 2008; Gavini et al., 2011; Maestrelli et al., 2004). Chitosan is also characterized by the ability to reversibly open tight junctions, which is associated with a potential increase in the transcellular transport of drugs across the olfactory mucosa (Durhia et al, 2010). Nasal formulations obtained in the presence of water have drawbacks, such as the risk of chemical and physical instability and microbiological growth. In addition, the residence time of the liquid formulation in the nasal cavity is short, as the liquid is often rinsed into the gastrointestinal tract (GIT) or out of the nose (Kublik and Vidgren, 1998). These disadvantages can be overcome by using powder-based formulations (Marttin et al., 1997; Rassu et al., 2015b).

The purpose of the present work was first to demonstrate that UDCA-AZT can

permeate and remain in macrophages more efficiently than its parent drug AZT and then to prepare microspheres based on chitosan chloride in order to increase the nose-to-brain delivery of UDCA-AZT by using a particulate formulation that is suitable for nasal administration. The characterization of microparticles was performed *in vitro* and *in vivo*. All *in vitro* and *in vivo* measurements performed for the loaded microparticles were also performed for a parent physical mixture of chitosan chloride and UDCA-AZT in order to verify the efficacy of the microparticulate system for the brain delivery of the prodrug.

## 2. Materials and methods

### *2.1. Materials*

The prodrug UDCA−AZT was synthesized as described previously (Dalpiaz et al., 2012). Chitosan chloride (Protasan UP CL 113, molecular weight and degree of deacetylation of 160,000 g/mol and 83%, respectively) was purchased from FMC BioPolymer AS (Drammen, Norway). Dow Corning 345, which is a blend of polydimethylcyclosiloxane, was obtained from Dow Corning (Brussels, Belgium). AZT, 7-n-propylxanthine (7n-PX), and bovine serum albumin (BSA) were obtained from Sigma Aldrich Italy (Milan, Italy). Methanol, acetonitrile, ethyl acetate and water were high performance liquid chromatography (HPLC) grade and obtained from Sigma Aldrich Italy. Monopowder P® insufflators were furnished by Valois Dispray (Mezzovico, Switzerland). Male Wistar rats were purchased from Harlan SRC (Milan, Italy). All other reagents and solvents were of analytical grade (Sigma-Aldrich).

### *2.2. Uptake of AZT and UDCA-AZT in macrophages*

The J774A.1 murine macrophage cell line was obtained from the American Tissue Type Culture Collection (LGC Standards, Milan, Italy). J774A.1 macrophages were grown as adherently cultured cells in Dulbecco's modified Eagle's medium + Glutamax supplemented with 10% fetal bovine serum (FBS), 100 U/mL penicillin, and 100 µg/mL streptomycin at 37 °C. All cell culture reagents were provided by Invitrogen (Life Technologies, Milan, Italy). The employed method is reported in detail in the Supplementary material. Briefly, a total of $5\times10^5$ cells J774A.1 cells were seeded in 12-well culture plates, and when semi-confluent, the cells were exposed to 100 µM AZT and 10 or 100 µM UDCA-AZT in growth medium for 30 min. At the end of the treatment, the cells were washed and lysed. The cell lysates were dried under a nitrogen stream, resuspended in methanol and centrifuged to remove cell debris. The supernatant (10 µl) was used to measure the levels of AZT and UDCA-AZT via HPLC analysis. All of the values obtained from experiments with J774A.1 cells are the mean of three independent experiments.

### *2.3. Toxicity texts (MTT assay)*

J774A.1 cells were seeded in 96-well plates at a density of 8,000 cells per well and reached an optimal population density within 48-72 h. The cells were then incubated for 15, 30 and 60 min in 200 µL of culture medium in the presence and absence of 100 µM UDCA-AZT. At the end of the time-course, the incubation medium was removed and replaced with 200 µL of fresh culture medium, and 20 µL of 3-(4,5-dimethylthiazol-2-yl)-2,5-diphenyltetrazolium bromide (MTT) stock solution (5 mg/mL) were added to each well and incubated at 37 °C for 4 h. A negative control of 20 µL of the MTT stock solution added to 200 µL of medium alone was included. Then, 100 µL of DMSO were added to each well and incubated at 37 °C for 2 h in an orbital shaker incubator. Finally, the absorbance of each well

was measured at 570 nm using a microtiter plate reader.

### *2.4. Preparation of loaded and unloaded chitosan microspheres*

Chitosan microspheres containing UDCA−AZT (named CP) were prepared using the spray-drying method. Chitosan chloride (400 mg) was dissolved in water (15 mL), whereas UDCA−AZT (100 mg) was dissolved in methanol (35 ml). The drug solution was dispersed into chitosan one (solid concentration: 1% w/v of UDCA−AZT and chitosan). Due to the very low solubility of the drug, a fine suspension was obtained and spray-dried using a mini spray-dryer equipped with a high performance cyclone (Büchi B-191, Büchi Labortechnik AG, Flawil, Switzerland) and with a 0.7 mm two-fluid nozzle. The following standard operating conditions were utilized: inlet and outlet temperature, 100 °C and 73 °C, respectively; spray flow rate, 500 L/h; pump setting, 8% (2.00 mL/min); and aspirator setting, 90%. Aqueous solutions of chitosan chloride (0.8 % w/v) were sprayed under the same conditions to obtain drug-free microspheres (CH). The microparticles were stored in a desiccator at room temperature.

### *2.5. HPLC analysis*

The prodrug UDCA−AZT and its hydrolysis product AZT were quantified using HPLC. The chromatographic apparatus consisted of a modular system (model LC-10 AD VD pump and model SPD-10A VP variable wavelength UV−vis detector; Shimadzu, Kyoto, Japan) and an injection valve with a 20 μL sample loop (model 7725; Rheodyne, IDEX, Torrance, CA, USA). Separations were performed at room temperature on a 5 μm Hypersil BDS C-18 column (150 mm × 4.6 mm i.d.; Alltech Italia Srl, Milan, Italy) equipped with a guard column. Data acquisition and processing were accomplished with a personal computer using

CLASS-VP Software, version 7.2.1 (Shimadzu Italia, Milan, Italy). The detector was set to 260 nm. The mobile phase consisted of a mixture of water and methanol that was regulated by a gradient profile programmed as follows: isocratic elution with 20% (v/v) MeOH in $H_2O$ for 10 min; a 1-min linear gradient to 75% (v/v) MeOH in $H_2O$; and the mobile phase composition was then maintained at 75% MeOH for 10 min. After each cycle, the column was conditioned with 20% (v/v) MeOH in $H_2O$ for 10 min. The flow rate was 1 mL/min. The xanthine derivative 7n-PX was employed as an internal standard for the analysis of rat blood (see below). The retention times for 7n-PX, AZT and the prodrug UDCA−AZT were 6.5, 8.4, and 19.6 min, respectively. The HPLC assay of UDCA-AZT alone was performed isocratically with 80% (v/v) MeOH in $H_2O$. In this case, the retention time of UDCA-AZT was 4.8 min. The chromatographic precision was evaluated (see Supplementary material).

### *2.6. Characterization of microspheres*

The prepared microspheres were characterized in terms of production yield, drug content and encapsulation efficiency, particle size and particle size distribution, particle morphology, true density and water uptake capacity.

#### *2.6.1. Production yields*

The production yields (YP) were calculated as a percent weight of microspheres obtained with respect to the initial amounts of UDCA−AZT and chitosan that were employed for the preparation of the feed suspension.

#### *2.6.2. UDCA−AZT content in CP*

The UDCA-AZT content in the microparticulate powders was determined. The microparticles (approximately 0.95 mg) were accurately weighed and dissolved in 3 ml of

water to which 300 µl of 0.2% $H_3PO_4$ was added; the final volume of the solution was adjusted to 10 mL with methanol. Then, 10 µL of the filtered solutions (0.45 µm) were injected into the HPLC system for the UDCA-AZT assay. The drug loading and entrapment efficiency were calculated according to equations 1 and 2 (Rassu et al., 2014; see Supplementary material).

All of the obtained values are the mean of four independent experiments.

*2.6.3. Particle size measurement*

The size and size distribution of the microspheres were analyzed via the light diffraction method using a Coulter LS 100Q (Beckman Coulter Particle Characterization, Miami, FL, USA). A sample (2 mg) of unloaded and drug-loaded microspheres was suspended in silicon oil, sonicated for approximately 3 s and analyzed. The reported results are the averages of triplicate averages. For comparison, a test was also performed on the physical mixture containing UDCA−AZT and chitosan chloride (87:13 w/w) (MIX) that was prepared by geometric dilution using an agate mortar pestle, as well as on chitosan chloride and UDCA-AZT alone, before and after grinding.

*2.6.4. Particle morphology*

The shape and surface characteristics of the powders were studied using scanning electron microscopy (VP-SEM; Zeiss EVO40XVP, Arese, Milan, Italy). The samples were placed on double-sided tape that had previously been secured to aluminum stubs and then analyzed under an argon atmosphere at an 18 kV acceleration voltage after gold sputtering.

*2.6.5. True Density*

The true density of the microspheres was measured via helium pycnometry (Micromeritics Accupyc II 1340 Analysis system, Peschiera Borromeo, Italy) at 21 °C

(Gavini et al., 2012). The density (ρ) of the powder was determined in triplicate for each batch.

*2.6.6. Determination of water uptake capacity*

Investigations of the water uptake capability of CP and CH were carried out using a modified Enslin apparatus, as described previously by Rassu et al., 2009. Briefly, the dried microspheres were spread uniformly on the filter paper, which was previously soaked with phosphate buffer, pH 6.5. The volume of fluid absorbed from the microspheres during the time of the experiment (0 to 60 min) was recorded. The values (mean of at least 3 experiments) were expressed as µl of fluid absorbed per gram of microspheres during the time of the experiment. For comparison, the test was also performed using MIX.

## *2.7. In vitro release and dissolution studies*

The release tests were performed using the flow-through dissolution method (European Pharmacopoeia, Apparatus 4), with a modified glass cell that is useful for organic solvents (described in the Supplementary material). The CP formulation (20 mg) was placed into the glass cell. The dissolution medium was warmed to 37±0.1 °C and introduced through the bottom of the cell to obtain a suitable continuous flow. A methanol-water blend (70-30 v/v) was used as the dissolution medium. The test solution (10 µL) was analyzed via HPLC to evaluate the amount of UDCA-AZT released from the microspheres, which was calculated as a percentage of the initial amount of UDCA−AZT incorporated into the microspheres prior to the dissolution test. For comparison, the test was also performed using MIX. All experiments were performed with at least three replicates.

## *2.8. In vivo UDCA-AZT administration and quantification*

Male Wistar rats (200–250 g) were anesthetized during the experimental period and received a femoral intravenous infusion of 0.1 mg/mL of UDCA-AZT dissolved in a medium constituted by 20% (v/v) DMSO and 80% (v/v) physiologic solution, at a rate of 0.2 mL/min for 10 min. At the end of the infusion and at fixed time points, blood samples (100 μL) were collected and CSF samples (50 μL) were withdrawn using the cysternal puncture method described by van den Berg et al. (2002), which requires a single needle stick and allows the collection of serial (40–50 μL) CSF samples that are virtually blood-free (Dalpiaz et al., 2014). A total volume of approximately 150 μL of CSF was collected during the experimental session. Four rats were employed for femoral intravenous infusions. The CSF samples (10 μL) were immediately injected into the HPLC system for AZT and UDCA-AZT detection. The blood samples were hemolysed immediately after their collection with 500 μL of ice cold water, and 50 μL of 10% sulfosalicylic acid and 100 μL of internal standard (30 μM 7n-PX) were then added. The samples were extracted twice with 1 mL of water-saturated ethyl acetate, and after centrifugation, the organic layer was reduced to dryness under a nitrogen stream. Two hundred microliters of a water-methanol mixture (70:30 v/v) were added, and after centrifugation, 10 μL were injected into the HPLC system for AZT and UDCA-AZT detection.

The precision of the analytical method was determined (see Supplementary material). The *in vivo* half-life of AZT in the blood was calculated by nonlinear regression (exponential decay) of concentration values in the time range within 3 h after infusion and confirmed by linear regression of the log concentration values versus time.

Nasal administration of UDCA-AZT was performed on anesthetized rats laid on their backs, following two main procedures. The first procedure consisted of the introduction of 50 μL of an aqueous suspension of UDCA-AZT (2 mg/mL) into each nostril, as described

previously (Dalpiaz et al., 2014). After administration, blood (100 μL) and CSF samples (50 μL) were collected at fixed time points and analyzed using the same procedures described above. Four rats were employed for nasal administration of the UDCA-AZT suspension.

The second procedure was based on the insufflation of CP microparticles into each nostril of anaesthetized rats using single dose Monopowder P® insufflators (Valois Dispray SA, Mezzovico, Switzerland). These devices were constituted by a pump, a nasal adapter and a solid formulation reservoir (Sacchetti et al., 2002). The insufflators were loaded with approximately 0.8 mg of UDCA-AZT-loaded microparticles (corresponding to approximately 100 μg of UDCA-AZT), or with approximately 0.8 mg of the corresponding physical mixture (MIX). The rats received this amount in each nostril. The amount of powder emitted during administration was determined based on the difference between the insufflator weights before and after each insufflation. After administration, blood (100 μL) and CSF samples (50 μL) were collected at fixed time points and analyzed using the same procedures described above. Four rats were employed for nasal administration of the microparticulate powder.

All *in vivo* experiments were performed in accordance with the guidelines issued by the Italian Ministry of Health (D.L. 116/92 and D.L. 111/94-B), the Declaration of Helsinki, and the Guide for the Care and Use of Laboratory Animals as adopted and promulgated by the National Institute of Health (Bethesda, Maryland, USA). The protocols for all *in vivo* experiments were approved by the Local Ethics Committee (University of Ferrara, Ferrara, Italy). All efforts were made to reduce the number of animals and their suffering.

The areas under the concentration curves of UDCA-AZT in the CSF (AUC, $\mu g\ mL^{-1}$ min) were calculated using the trapezoidal method. The *in vivo* half-life of UDCA-AZT in the CSF was calculated by linear regression of the log concentration values versus time between 1 and 3 h after nasal administration of the loaded microparticles. All calculations were performed using the computer program Graph Pad Prism (GraphPad Software, Incorporated, La Jolla, CA, USA).

### 2.9. *Statistical analysis*

Statistical comparisons of the amounts of water uptake of the powder samples and the UDCA-AZT $C_{max}$ and AUC values obtained in the CSF of rats were made using the Student's t test or one-way ANOVA (GraphPad Prism). P values <0.05 were considered to be statistically significant.

## 3. Results

### 3.1. *Uptake of AZT and UDCA-AZT in macrophages*

The incubation of 100 μM zidovudine or its prodrug with the macrophages for 30 min allowed us to detect 0.054±0.007 nmoles of AZT and 1.12±0.16 nmoles of UDCA-AZT in $10^6$ cells, as reported in Fig. 1. The amount of AZT detected in the cells after incubation with UDCA-AZT for 30 min was 0.081±0.009 nmoles/$10^6$ cells (Fig. 1). The cell counter measured the volume of macrophages as 1.7±0.1 pL; as a consequence, the amount of AZT released by the macrophages after incubation with 100 μM UDCA-AZT incubation corresponds to a concentration of 47±5 μM. No toxicity was observed for cells incubated with 100 μM UDCA-AZT. These data indicate not only that the prodrug is able to permeate and remain in the macrophages with an efficiency twenty times higher than that of its parent drug (P<0.001) but also that the macrophages hydrolyze the prodrug, facilitating intracellular AZT release (Fig 1). Moreover, the incubation of macrophages with 10 μM UDCA-AZT allowed us to detect 0.21±0.03 nmoles of the prodrug in $10^6$ cells (Fig 1). In this case, the AZT amounts were lower than the limit of detection of the analytical system. Therefore, the

ability of UDCA-AZT to elude the AET systems (Dalpiaz et al., 2012) appears to be useful for inducing uptake into macrophages. According to the data reported in Fig. 1, the presence of the prodrug in the CSF should allow its permeation and permanence in the macrophages, therefore making the prodrug an efficient carrier for AZT.

### *3.2. Characterization of microspheres*

#### *3.2.1. Production yields*

The spray-drying technique proved to be suitable for preparing loaded and unloaded chitosan microparticles; in fact, these microparticles were obtained with good production yields of between 61.7% (CP) and 64.7% (CH). Generally, the yields obtained with the spray-drying at laboratory scale with conventional spray-dryers are in the range of 20–70% due to the loss of product on the walls of the drying chamber and the low capacity of the cyclone to separate fine particles (Giunchedi et al., 2000; Sosnik and Seremeta, 2015). However, the yield strongly depends on the work scale; the yield is high in larger scale setups because large batch sizes and separators (e.g., filter systems) are used.

#### *3.2.2. UDCA−AZT content in CP*

The amount of encapsulated UDCA−AZT in the CP sample was found to be 13±0.3% (w/w), showing that chitosan, which is characterized by hydrophilic properties, was able to encapsulate the lipophilic prodrug with a good encapsulation efficiency (64.9±1.5%).

#### *3.2.3. Particle size measurement*

Table 1 reports the volume-surface diameters ($d_{vs}$) obtained for the loaded (CP) and unloaded microparticles (CH), for MIX and for chitosan chloride and UDCA-AZT before and after grinding using an agate mortar and pestle. The loading of UDCA−AZT into chitosan

microparticles caused an increase in the particle size: CP microspheres had a $d_{vs}$ of 3.59±0.1 μm in comparison to a $d_{vs}$ of 2.32±0.01 μm for CH ($P<0.0001$). Furthermore, the presence of the drug resulted in a change in the particle size distribution: loaded microparticles showed a larger curve than drug-free microspheres (Fig. 2 up). In particular, CH showed a Gaussian curve while the CP curve appeared to be leptokurtic, right skewed and wide, with the presence of small shoulders.

MIX had a $d_{vs}$ of 6.11±0.022 μm, which was significantly higher than the values obtained for microspheres ($P<0.001$) and UDCA-AZT alone but significantly lower than the value obtained for chitosan chloride alone, which were both analyzed after grinding. The grinding of the drug and the polymer in an agate mortar reduced the particle size and shifted the size distributions to lower values (Fig. 2, lower panel). In fact, the $d_{vs}$ of chitosan chloride changed from 19.98±0.24 μm to 12.67±0.819 μm due to aggregate breaking. The size reduction of UDCA-AZT crystals was even more pronounced: the $d_{vs}$ decreased from 23.33±0.06 μm to 5.12±0.018 μm after grinding.

*3.2.4. Particle morphology*

Fig. 3A presents an SEM image of MIX obtained by geometric dilution using an agate mortar and pestle. This picture reveals not only particles characterized by a round morphology and a relatively smooth surface but also the presence of fragments characterized by an irregular shape. For comparison, Figs. 3B and 3C present SEM images of chitosan chloride and UDCA-AZT, respectively, which were ground using an agate mortar and pestle. Fig. 3B shows particles characterized by a round morphology and a smooth surface. These morphologic characteristics did not appear to be significantly different from those of chitosan chloride before grinding, as evidenced by the SEM image presented in Fig. 3E. The SEM picture of ground UDCA-AZT, Fig. 3C, showed fragments characterized by an irregular shape (details are evident in the SEM image reported in Fig. 3D) and a high aptitude to

aggregate. These morphologic characteristics appeared to be significantly different from those of the prodrug UDCA-AZT before grinding, as evidenced in Fig. 3F, where fragments of an irregular shape are shown to be characterized by diameters at least one order of magnitude higher than those of the ground UDCA-AZT particles. Taking into account these aspects, we can conclude that the SEM image of the physical mixture of chitosan chloride and UDCA-AZT (Fig. 3A) allows us to discriminate its two components; in particular, the particles with a round morphology can be attributed to chitosan chloride, whereas the fragments of irregular shape can be attributed to UDCA-AZT.

Figs. 4A and 4B present SEM images of CP, which is constituted by the loaded UDCA-AZT microparticles based on chitosan chloride. The pictures reveal the presence of spherical particles characterized by a smooth surface and several fragments characterized by an irregular shape and high porosity, similar to spongy balls, with some degree of aggregation. For comparison, a SEM image of the unloaded microparticles (CH) (Dalpiaz et al., 2008) reveals their round shape and smooth surfaces. Taking into account these aspects, we can hypothesize that the spherical particles presented in images 3A and 3B are constituted by unloaded chitosan chloride, whereas the spongy balls were obtained from the interaction between chitosan chloride and UDCA-AZT, which gave rise to the highly porous structures.

*3.2.5. True density*

The true density of the microspheres was 1.48±0.02 g/cm$^3$, which is comparable to the ρ of nasal microspheres (Gavini et al., 2012).

*3.2.6. Determination of water uptake capacity*

Fig. 5 shows the water uptake of both loaded and unloaded formulations. The drug-free formulations absorbed a greater amount of water than the loaded microparticles. Drug loading decreased the water absorption capability of chitosan microspheres ($P<0.05$). UDCA−AZT

and the chitosan chloride physical mixture also exhibited water uptake capabilities stronger than that of CP but weaker than that of CH after 15 to 60 min ($P<0.05$).

### *3.3. In vitro release and dissolution studies*

The dissolution and release studies of UDCA−AZT were performed in a MeOH/$H_2O$ (70:30, v/v) mixture. The employment of methanol as a cosolvent was necessary to increase the low solubility of the prodrug in water (0.0030±0.0001 mg/ml; Dalpiaz et al., 2012), thus ensuring sink conditions.

Fig. 6 reports the release profile of UDCA−AZT from the loaded CP sample. The release pattern is compared with that of UDCA-AZT dissolution from its physical mixture with chitosan chloride. The dissolution rate of the prodrug included in MIX appeared to be significantly lower than that of UDCA-AZT loaded in the CP sample. Indeed, after 2 h of incubation, 38.4±1.6% of the prodrug loaded in the dissolution apparatus appeared to have dissolved, whereas in the case of CP loaded microparticles, the amount of dissolved UDCA-AZT was 86.2±3.4%. As a consequence, the dissolution half-life of UDCA-AZT loaded in CP sample appeared to be approximately 15 min, whereas for the prodrug in the physical mixture (MIX), the dissolution half-life was greater than 2 h. These profiles suggest that the employment of the CP sample as a nasal formulation should be appropriate, as this formulation is able to release the prodrug UDCA-AZT in a relatively short time, allowing potentially rapid absorption of the prodrug after the administration of the microparticles.

### *3.4. In vivo UDCA-AZT administration*

Taking into account the fact that the CP microparticles were characterized not only by a satisfactory encapsulation efficiency but also by the ability to induce relatively rapid

dissolution of UDCA−AZT, we tested these microparticles for nasal administration of the prodrug in order to verify potential uptake in the CNS. The nasal administration of UDCA−AZT was performed using three different formulations: (i) a suspension of the raw UDCA-AZT powder in water, (ii) the powder constituted by loaded CP microparticles and (iii) for comparison, the parent physical mixture of chitosan chloride and UDCA-AZT (87:13 w/w). The results were compared with those obtained after the intravenous infusion of UDCA−AZT into rats.

### *3.4.1. Intravenous administration of UDCA−AZT*

The prodrug was undetectable in rat blood samples following intravenous infusion. This result is in agreement with the very fast hydrolysis of UDCA−AZT in rat blood at 37 °C (Dalpiaz et al., 2012). Significant amounts of AZT were therefore detected following the intravenous administration of the prodrug, as evidenced in Fig. 7. In particular, after the infusion of 0.200 mg of UDCA−AZT into the rats, the AZT concentration in the bloodstream was 4.50±0.31 μg/mL. This concentration decreased over time with apparent first order kinetics, as confirmed by the linearity of the semilogarithmic plot reported in the inset of Fig. 7 ($n = 9$, $r = 0.990$, $P<0.0001$), and a half-life of 60.4±3.8 min. These data are in good agreement with those obtained from previous studies of *in vivo* UDCA-AZT pharmacokinetics (Dalpiaz et al., 2014). No AZT or UDCA−AZT was detected in the CSF within 180 min after the intravenous administration of UDCA−AZT.

### *3.4.2. Nasal Administration of UDCA−AZT*

The nasal administration of pure UDCA-AZT as a water suspension did not allow us to obtain detectable amounts of AZT or the prodrug in the blood or in the CSF, respectively, within 180 min of administration, as reported previously (Dalpiaz et al., 2014). In contrast, the nasal administration of the powders constituted by MIX or by the CP microparticles (0.8 mg,

approximately 100 μg of UDCA−AZT in each nostril) produced detectable amounts of UDCA−AZT in the CSF of the rats, as reported in Fig. 8. In particular, the UDCA−AZT $C_{max}$ was obtained after 60 min, with a value of 1.96±0.29 μg/mL (3.1±0.4 μM), after nasal administration of the mixture.

The nasal administration of the same amount of CP microparticles increased the rate of uptake of the prodrug into the CSF of rats. Indeed, the UDCA−AZT $C_{max}$ was obtained at 60 min, with a value of 2.99±0.31 μg/mL (4.7±0.5 μM), which was significantly higher than the $C_{max}$ value obtained for the MIX sample ($P < 0.001$).

No AZT was detected in the bloodstream or in the CSF within 180 min after nasal administration of the powders constituted by MIX or the CP microparticles.

The areas under the concentration (AUC) curve values obtained for UDCA−AZT in the CSF after the nasal administration of MIX and CP microparticles (Fig. 8) were 201.39±13.51 μg $mL^{-1}$ min and 354.4±13.3 μg $mL^{-1}$ min, respectively. The ratio between the AUC of the CP sample and the AUC of the mixture was 1.76, indicating that the nasal formulation constituted by the CP microparticles allowed an uptake of UDCA−AZT into the CSF that was 76% higher than that obtained after the administration of the parent mixture ($P< 0.001$).

The UDCA-AZT concentration in the CSF after nasal administration of CP microparticles decreased over time with apparent first order kinetics, as confirmed by the linearity of the semilogarithmic plot reported in the inset of Fig. 8 ($n = 4$, $r = 0.998$, $P < 0.05$), and a half-life of 80.4±9.2 min.

## 4. Discussion

Although antiretroviral nucleoside derivatives are largely used against HIV infection for their efficacy at the peripheral level, the total eradication of this virus from the body is

currently difficult to achieve. Indeed, antiretroviral drugs are unable to reach the CNS (Kaufmann and Cooper, 2000; Strazielle, 2003); in contrast, the CNS is easily reached by HIV through infected monocytes (Davis et al., 1992; Gray et al., 1996) that differentiate into macrophages and microglia in the brain (Rausch and Stover, 2001). Therefore, the CNS and those macrophages constitute sanctuaries for HIV, where drug resistance is induced and from which the periphery can be re-infected (Cunningham et al., 2000; Kolson and Gonzalez-Scarano, 2000). These phenomena are attributed primarily to the expression of AETs on the membranes of macrophages (Chaudhary et al., 1992; Neyfakh et al., 1989) and blood brain barrier (BBB) cells (Namanja et al., 2012; Pavan and Dalpiaz 2011), whose activity prevents the penetration of antiretroviral drugs into HIV sanctuaries.

Among numerous nucleoside antivirals, AZT was the first to be approved and remains the most widely used for the treatment and prophylaxis of HIV/AIDS (Hughes, 2015). Unfortunately, long-term clinical use of AZT is associated with significant side effects, but despite these drawbacks, AZT is considered to be one of the more potent inhibitors of the HIV DNA polymerase (reverse transcriptase) (Arts and Hazuda, 2012; Golan et al., 2011). Currently, tenofovir (TDF) is known to be a more potent and less toxic antiretroviral (ARV) drug than AZT; however, a higher virological failure rate was observed after a clinical TDF-containing ARV regimen in comparison to AZT-containing ARV therapy (Tang et al., 2012).

AZT activity in the CNS appears to be necessary not only in the brain tissue but also in the CSF subarachnoid spaces that contain macrophages and constitute the only site of HIV replication in the brain (Cunningham et al., 1997; Ghersi-Egea et al., 1996). It is therefore important to obtain formulations that are able to target AZT to the CSF, but it is equally important to induce the ability of AZT to elude the AET systems in order to avoid its extrusion from the CNS and the associated macrophages. In this regard, we know that the prodrug UDCA-AZT, which was obtained by the conjugation of AZT to ursodeoxycholic acid (UDCA), is able to elude the AET systems (Dalpiaz et al., 2012). Moreover, the results

reported in this paper demonstrate for the first time that the prodrug UDCA-AZT is more efficient than AZT in permeating and remaining inside the murine macrophage-like J774A.1 cell line, which is commonly used as model system for studying the internalization process of macrophages (Wang et al., 2012). Human cells can be used for *in vitro* studies of inflammation and infection, and many similarities between immortalized human monocytic cell lines (e.g., U937 and THP-1) and primary human blood monocytes have been reported (Yagil-Kelmer et al., 2004). However, these immature cells often require the addition of stimulant factors to promote their differentiation to a mature, adherent phenotype (Shelley et al., 2002). This requirement complicates the study of inflammatory outcomes related to these cell types, as stimulant factors exert specific effects on cellular behavior. Additionally, maturation protocols vary across studies. In contrast, murine cell lines offer the advantage of an immortalized, relatively stable, mature, adherent macrophage phenotype. The murine cell lines J774A.1, RAW 264.7 and IC-21 exhibit the maturity markers F4/80 and Mac-1, indicating their macrophage-like phenotypes, and have been used as models of macrophage activation in numerous studies (Chamberlain et al., 2009). As an example, J774 mouse macrophages have been successfully used to demonstrate the uptake of azidothymidine triphosphate (AZT-TP)-loaded nanoparticles and the related efficient delivery of AZT-TP into the cell cytoplasm (Giacalone et al., 2013).

Moreover, our results demonstrate that the prodrug UDCA-AZT is hydrolyzed in macrophages, facilitating intracellular AZT release. Interestingly, no toxicity was observed in the macrophages during their incubation with UDCA-AZT. We demonstrated previously that this prodrug is not a substrate of human AETs (Dalpiaz et al., 2012). This result suggests that UDCA-AZT should not be subject to efflux from human macrophages. Furthermore, AZT is known to induce anti-HIV activity in the HTLV-1-transformed cell line MT-4, which is highly susceptible to and permissive for HIV infection (Magnani et al., 1996), thus suggesting that AZT is able to induce anti-HIV activity in human macrophages.

It is important to note that the prodrug UDCA-AZT is quickly hydrolyzed in whole blood, so intravenous administration is not suitable for its permeation across the BBB. Indeed, following this type of administration, we detected only AZT, which exhibited concentration values that decreased over time with a half-life of approximately 1 h. No AZT or UDCA−AZT were detected in the CSF of rats after intravenous administration. In contrast, the nasal administration of this prodrug appears promising for achieving uptake into the CNS and particularly the CSF. We demonstrated that the nasal administration of chitosan-based microparticles can induce the selective uptake of neuroactive agents into the CSF of rats, probably by promoting drug permeation across the olfactory nasal mucosa (Dalpiaz et al., 2008; Gavini et al., 2011; Rassu et al., 2015a). Very recently, the poor water solubility of UDCA-AZT encouraged us to encapsulate this prodrug in solid lipid microparticles (Dalpiaz et al., 2014). In particular, the nasal administration of UDCA-AZT loaded in stearic acid-based microparticles induced the selective uptake of the prodrug into the CSF of rats, with amounts of up to approximately 0.4 µg/ml within 60 min after administration (Dalpiaz et al., 2014). These amounts increased (up to approximately 1.50 µg/mL within 120 min after administration) when the same quantity of microparticles were administered nasally as a water suspension in the presence of chitosan chloride (Dalpiaz et al., 2014). This result was attributed to the good mucoadhesive properties of chitosan (Dalpiaz et al., 2008) and to its ability to transiently open the tight junctions in the epithelial membranes (Dodane et al, 1999; Illum et al., 1994).

Nasal formulations obtained in the presence of water can be associated with the risk of chemical and physical instability and microbiological growth. Moreover, in the nasal cavity, liquid formulations are often rinsed into the GIT or out of the nose, so their residence time is generally short (Kublik and Vidgren, 1998). These disadvantages can be overcome by using powder-based formulations (Marttin et al., 1997; Rassu et al., 2015b). For this reason, we prepared microspheres based on chitosan chloride in order to increase the nose-to-brain

delivery of UDCA-AZT. The efficacy of the microparticulate system for the brain delivery of the prodrug was verified by comparing the properties of the microparticles with those of their parent physical mixture, which was obtained by geometrical dilution of the components using an agate mortar and pestle. The grinding process induced a reduction of the $d_{vs}$ diameters of chitosan chloride and the UDCA-AZT particles. The chitosan chloride particles were characterized by a round morphology and a relatively smooth surface before and after grinding, whereas UDCA-AZT appeared as fragments with an irregular shape. These two different morphological characteristics were distinctly apparent in the SEM picture of the physical mixture, where small irregular fragments of UDCA-AZT appeared on the surface of larger and rounder chitosan chloride microspheres.

The spray-drying process allowed us to obtain unloaded microparticles of chitosan chloride (CH) with the "classical" round morphology and a small $d_{vs}$ diameter. The loaded microparticles (CP) evidenced a slight increase in size and a morphology characterized by spherical particles mixed with fragments of irregular shape and high porosity, similar to spongy balls, with some degree of aggregation. We can conclude that the spherical particles are attributable to pure chitosan chloride that has not interacted with UDCA-AZT during the spray-drying process, whereas the "spongy balls" were obtained by a combination of the prodrug with polymer, inducing the formation of the highly porous structures. The different degrees of water solubility between UDCA-AZT and chitosan can justify these characteristics of the CP formulation. The description of the CP formulation's morphology appears to be consistent with the observed dissolution and water uptake profiles. Indeed, we observed that the dissolution rate of UDCA-AZT from the CP sample was significantly higher than that of the parent physical mixture. This phenomenon can be attributed to the highly porous structures observed in the CP sample, which allows a faster dissolution of UDCA-AZT with respect to its fragments included in MIX. Moreover, as demonstrated previously by Gavini et al. (2011), water soluble chitosans, such as salts, are more able to completely amorphize

poorly soluble drugs into the polymer matrix compared to the chitosan base; as a consequence, the dissolution rate and bioavailability of poorly soluble drugs improve.

Moreover, we observed that the water uptake rate of the CH sample was significantly reduced if chitosan chloride was mixed with UDCA-AZT, but a drastic decrease was observed in the case of the CP sample. The presence of UDCA-AZT, which is a very poorly water soluble molecule, in the physical mixture can explain its reduction of water uptake with respect to the CH sample, but the drastic reduction observed for the CP microparticles can be attributed to their porous structures, in which the presence of the prodrug and chitosan chloride together contributed to dramatically reducing the water uptake aptitude of the polymer.

Therefore, the CP sample appeared to be a valuable formulation for the nasal administration of UDCA-AZT. In particular, we hypothesized that the size and density of the microparticles should induce their deposition on the nasal mucosa, which should not be dehydrated by their presence, given the poor the water uptake of this sample. Moreover, the ability of the loaded microparticles to increase the dissolution rate of UDCA-AZT suggested their potential aptitude for inducing prodrug permeation across the nasal mucosa, a phenomenon that is probably potentiated by the ability of chitosan to transiently open tight junctions (Illum et al., 2015).

The nasal administration of raw UDCA−AZT to rats did not produce any detectable levels of UDCA−AZT or AZT in the bloodstream or the CSF, whereas the nasal administration of the CP sample and its parent physical mixture allowed us to obtain relatively high levels of UDCA-AZT in the CSF of rats 60 min after administration. The relative bioavailability of the CP sample was 176% of that of its parent physical mixture ($P<0.001$). No AZT was detected in the bloodstream of rats after nasal administration of the CP sample and its parent physical mixture, confirming the existence of a direct nose−CNS pathway for this prodrug (Dalpiaz et al., 2014). Our results demonstrate that the role of

chitosan in inducing selective UDCA-AZT uptake into the CSF is potentiated when the prodrug is formulated as a microparticulate system by spray-drying. This phenomenon is illustrated in Fig. 9, which presents a comparison of the AUC values obtained in the CSF after nasal administration of the same dose of UDCA-AZT (200 μg) to rats using different formulations (i.e., the solid lipid microparticles (SLMs), their water dispersion in the presence of chitosan (SLMs + Ch), which was obtained previously by Dalpiaz et al. (2014), MIX and CP, which was described here). In particular, CP was able to induce an uptake of UDCA-AZT into the CSF of rats that was 1.8, 3.2 and 18.6 times greater than that of its parent physical mixture (MIX), the dispersion of solid lipid particles in the presence of chitosan (SLMs + Ch) and the SLMs in solid form, respectively.

To summarize, after nasal administration, chitosan microspheres induce the efficient uptake of UDCA-AZT into the CSF. We demonstrated previously that this prodrug is able to elude the AETs and avoid their inactivation (Dalpiaz et al., 2012); as a consequence, the ability of the prodrug to elude the AET systems can prevent its extrusion into the bloodstream and induce AZT transport in the macrophages located in the subarachnoid spaces of the CSF. Consistent with these findings, it was demonstrated previously that the nasal co-administration of AZT and probenecid (an inhibitor of AETs) increased AZT uptake into the CSF of rats (Seki et al., 1994).

Taking into account the observations that the UDCA-AZT $C_{max}$ obtained in the CSF after the nasal administration of the sample CP was approximately 5 μM and that the half-life of the prodrug in the CSF was approximately 90 min, we can hypothesize that multiple nasal administrations every 90 min will allow rats to obtain UDCA-AZT concentrations ranging between approximately 5 and 10 μM in their CSF (Bourne and Dittert, 1990). We demonstrated that the incubation of macrophages with 10 μM and 100 μM UDCA-AZT allowed us to detect prodrug amounts ranging from approximately 0.2 to 1 nmoles in $10^6$ cells. We also demonstrated that the AZT concentration in macrophages after incubation

with UDCA-AZT was 47 μM. AZT exhibits anti-HIV activity in the HTLV-1-transformed cell line MT4, with an $IC_{50}$ value of approximately 30 nM (Magnani et al., 1996), which is more than three orders of magnitude lower than the concentration of AZT that we detected in the macrophages after incubation with 100 μM UDCA-AZT. Therefore, it seems reasonable to deduce that incubation with 5 or 10 μM UDCA-AZT can allow the macrophages to attain AZT concentrations sufficient to induce anti-HIV activity. As a consequence, taking into account the aspects we described above, we predict that the amount of UDCA-AZT taken up in the CSF following the nasal administration of the loaded microparticles might be sufficient to achieve anti-HIV activity in the CNS.

## Conflicts of interest

The authors declare that they have nothing to disclose regarding funding or conflicts of interest relating to this manuscript.


## Acknowledgements

This research was supported by a grant from Ministero dell'Istruzione, dell'Università e della Ricerca (PRIN 2012).


## References


Arts, E.J., Hazuda, D.J., 2012. HIV-1 antiretroviral drug therapy. Cold Spring Harb. Perspect. Med. 2, a007161.

Bernkop-Schnürch, A., Dünnhaupt, S., 2012. Chitosan-based drug delivery systems. Eur. J. Pharm. Biopharm. 81, 463-469.

Bourne, D.W., Dittert, L.W., 1990. Pharmacokinetics, in: Banker, G,S, Rhodes, C.T. (Eds), Modern Pharmaceutics , Marcel Dekker INC, New York, pp. 91-142.

Casettari, L., Illum, L., 2014. Chitosan in nasal delivery systems for therapeutic drugs. J. Control. Rel. 190, 189-200.

Chamberlain, L.M., Godek, M.L., Gonzalez-Juarrero, M., Grainger, D.W., 2009. Phenotypic non-equivalence of murine (monocyte-) macrophage cells in biomaterial and inflammatory models. J. Biomed. Mater. Res. A. 88, 858-871.

Chaudhary, P.M., Mechetner, E.B., Roninson, I.B., 1992. Expression and activity of the multidrug resistance p-glycoprotein in human peripheral blood lymphocytes. Blood 80, 2735−2739.

Cho, W., Kim, M.S., Jung, M.S., Park. J., Cha, K.H., Kim, J.S., Park, H.J., Alhalaweh, A., Velaga, S.P., Hwang, S.J., 2014. Design of salmon calcitonin particles for nasal delivery using spray-drying and novel supercritical fluid-assisted spray-drying processes. Int. J. Pharm. 478, 288-296.

Cunningham, A. L., Naif, H., Saksena, N., Lynch, G., Chang, J., Li, S., Jozwiak, R., Alali, M., Wang, B., Fear, W., Sloane, A., Pemberton, L., Brew, B., 1997. HIV infection of macrophages and pathogenesis of AIDS dementia complex: interaction of the host cell and viral genotype. J. Leukocyte Biol. 62, 117−125.

Cunningham, P.H., Smith, D.G., Satchell,C., Cooper, D.A., Brew, B., 2000. Evidence for independent development of resistance to HIV-1 reverse transcriptase inhibitors in the cerebrospinal fluid. AIDS 14, 1949−1954.

Dalpiaz, A., Gavini, E., Colombo, G., Russo, P., Bortolotti, F., Ferraro, L., Tanganelli, S., Scatturin, A., Menegatti, E., Giunchedi, P., 2008. Brain uptake of an antiischemic agent by nasal administration of microparticles. J. Pharm. Sci. 97, 4889−4903.

Dalpiaz, A., Paganetto, G., Pavan, B., Fogagnolo, M., Medici, A., Beggiato, S., Perrone, D., 2012. Zidovudine and ursodeoxycholic acid conjugation: design of a new prodrug potentially able to bypass the active efflux transport systems of the central nervous system. Mol. Pharm. 9, 957−968.

Dalpiaz, A., Ferraro, L., Perrone, D., Leo, E., Iannuccelli, V., Pavan, B., Paganetto, G., Beggiato, S., Scalia, S., 2014. Brain uptake of a zidovudine prodrug after nasal administration of solid lipid microparticles. Mol. Pharm. 11:1550-1561.

Davis, L.E., Hjelle, B.L., Miller, V.E., Palmer, D.L., Llewellyn, A.L., Merlin, T.L., Young, S.A., Mills, R.G., Wachsman, W., Wiley, C.A., 1992. Early viral brain invasion in iatrogenic human immunodeficiency virus infection. Neurology 42, 1736−1739.

De Clercq, E., 2009. Anti-HIV Drugs: 25 compounds approved within 25 years after the discovery of HIV. Int. J. Antimicrob. Agents 33, 307−320.

Dodane, V., Khan, M.A., Merwin, J.R., 1999. Effect of chitosan on epithelial permeability and structure. Int. J. Pharm. 182, 21−32.

Fine, J.M., Forsberg, A.C., Renner, D.B., Faltesek. K.A., Mohan, K.G., Wong, J.C., Arneson, L.C., Crow, J.M., Frey. W.H. 2nd, Hanson. L.R., 2014. Intranasally-administered deferoxamine mitigates toxicity of 6-OHDA in a rat model of Parkinson′s disease. Brain Res. 1574, 96-104.

Fine, J.M., Renner, D.B., Forsberg, A.C., Cameron, R.A., Galick, B.T., Le, C., Conway, P.M., Stroebel, B.M., Frey, W.H. 2nd, Hanson, L.R., 2015. Intranasal deferoxamine engages multiple pathways to decrease memory loss in the APP/PS1 model of amyloid accumulation. Neurosci. Lett. 584, 362-367.

Finger, T.E., Jeor St., V.L., Kinnamon, J.C., Silver, W.L., 1990. Ultrastructure of substance P- and CGRP-immunoreactive nerve fibers in the nasal epithelium of rodents. J. Comp. Neurol. 294, 293-305.

Gavini, E., Rassu, G., Ferraro, L., Generosi, A., Rau, J.V., Brunetti, A., Giunchedi, P., Dalpiaz, A., 2011. Influence of chitosan glutamate on the ± intranasal absorption of rokitamycin from microspheres. J. Pharm. Sci. 100, 1488-1502.

Gavini, E., Rassu, G., Ciarnelli, V., Spada, G., Cossu, M., Giunchedi, P., 2012. Mucoadhesive drug delivery systems for nose-to-brain targeting of dopamine. J. Nanoneurosci. 2, 47-

55.

Ghersi-Egea, J. F., Finnegan, W., Chen, J. L., Fenstermacher, J. D., 1996. Rapid distribution of intraventricularly administered sucrose into cerebrospinal fluid cisterns via subarachnoid velae in rat. Neuroscience 75, 1271−1288.

Giacalone, G., Bochot, A., Fattal, E., Hillaireau, H., 2013. Drug-induced nanocarrier assembly as a strategy for the cellular delivery of nucleotides and nucleotide analogues. Biomacromolecules 14, 737-742.

Giunchedi, P., Gavini, E., Bonacucina, G., Palmieri, G.F., 2000. Tabletted polylactide microspheres prepared by a w/o emulsion-spray drying method. J. Microencapsul., 17, 711–720.

Gray, F., Scaravilli, F., Everall, I., Chretien, F., An, S., Boche, D., Adle-Biassette, H., Wingertsmann, L., Durigon, M., Hurtrel, B., Chiodi, F., Bell, J., Lantos, P., 1996. Neuropathology of aarly HIV-1 infection. Brain Pathol. 6, 1−15.

Golan, D. E., Tashjian A.H., Armstrong E.J., 2011. Principles of Pharmacology: The Pathophysiologic Basis of Drug Therapy, third ed. Lippincott Williams & Wilkins, Philadelphia.

Horvát, S., Fehér, A., Wolburg, H., Sipos, P., Veszelka, S., Tóth, A.; Kis, L., Kurunczi, A., Balogh, G., Kürti, L., Eros, I., Szabó-Révész, P., Deli, M. A., 2009. Sodium hyaluronate as a mucoadhesive component in nasal formulation enhances delivery of molecules to brain tissue. Eur. J. Pharm. Biopharm 72, 252−259.

Hughes, SH., 2015. Reverse transcription of retroviruses and LTR Retrotransposons. Microbiol. Spectr. 3, MDNA3-0027-2014.

Illum, L., Farraj, N.F., Davis, S.S., 1994. Chitosan as a novel nasal delivery system for peptide drugs. Pharm. Res. 11, 1186−1189.

Illum, L., 2000.Transport of drugs from the nasal cavity to the central nervous system. Eur. J. Pharm. Sci. 11, 1−18.

Illum, L., 2004. Is nose-to-brain transport of drugs in man a reality? J. Pharm. Pharmacol., 56, 3−17.

Johnson, NJ., Hanson, L.R., Frey, W.H., 2010. Trigeminal pathways deliver a low molecular weight drug from the nose to the brain and orofacial structures. Mol. Pharm. 7, 884−893.

Kaufmann, G.R., Cooper, D.A., 2000. Antiretroviral therapy of HIV-1 infection: established treatment strategies and new therapeutic options. Curr. Opin. Microbiol. 3, 508−514.

Kolson, D.L., Gonzalez-Scarano, F., 2000. HIV and HIV dementia. J. Clin. Invest. 106, 11−13.

Kublik, H., Vidgren, M.T., 1998. Nasal delivery systems and their effect on deposition and absorption, Adv. Drug Del. Rev. 29, 157–177.

Maestrelli, F., Zerrouk, N., Chemtob, C., Mura, P., 2004. Influence of chitosan and its glutamate and hydrochloride salts on naproxen dissolution rate and permeation across Caco-2 cells. Int. J. Pharm. 271, 257-267.

Magnani, M., Casabianca, A., Fraternale, A., Brandi, G., Gessani, S., Williams, R., Giovine, M., Damonte, G., De Flora, A., Benatti, U., 1996. Synthesis and targeted delivery of an azidothymidine homodinucleotide conferring protection to macrophages against retroviral infection. Proc. Natl. Acad. Sci. USA 93, 4403-4408.

Marttin, E., Romeijn, S.G., Verhoef, J.C., Merkus, F.W.H.M., 1997. Nasal absorption of dihydroergotamine from liquid and powder formulations in rabbits, J. Pharm. Sci. 86, 802–807.

Mistry, A., Stolnik, S., Illum, L., 2009. Nanoparticles for Direct nose to-brain delivery of drugs. Int. J. Pharm. 379, 146−157.

Namanja, H.A.; Emmert, D.; Davis, D.A.; Campos, C.; Miller, D.S., Hrycyna, C.A., Chmielewski, J., 2012. Toward eradicating HIV reservoirs in the brain: inhibiting P-glycoprotein at the blood-brain barrier with prodrug abacavir dimers. J. Am. Chem. Soc.

134, 2976–2980.

Neyfakh, A.A., Serpinskaya, A.S., Chervonsky, A.V., Apasov, S.G., Kazarov, A.R., 1989. Multidrug-resistance phenotype of a subpopulation of T-lymphocytes without drug selection. Exp. Cell Res. 185, 496−505.

Pavan, B., Dalpiaz, A., 2011. Prodrugs and endogenous transporters: are they suitable tools for drug targeting into the central nervous system? Curr. Pharm. Des. 17, 3560−3535.

Rassu, G., Gavini, E., Jonassen, H., Zambito, Y., Fogli, S., Breschi, M.C., Giunchedi, P., 2009. New chitosan derivatives for the preparation of rokitamycin loaded microspheres designed for ocular or nasal administration. J. Pharm. Sci. 98, 4852-4865.

Rassu, G., Nieddu, M., Bosi, P., Trevisi, P., Colombo, M., Priori, D., Manconi, P., Giunchedi, P., Gavini, E., Boatto, G., 2014. Encapsulation and modified-release of thymol from oral microparticles as adjuvant or substitute to current medications. Phytomedicine, 21, 1627–1632.

Rassu, G., Soddu, E., Cossu, M., Brundu, A., Cerri, G., Marchetti, N., Ferraro, L., Regan, R.F., Giunchedi, P., Gavini, E., Dalpiaz, A., 2015a. Solid microparticles based on chitosan or methyl-β-cyclodextrin: a first formulative approach to increase the nose-to-brain transport of deferoxamine mesylate. J. Contr. Rel. .201, 68–77.

Rassu, G., Soddu, E., Cossu, M., Gavini, E., Giunchedi, P., Dalpiaz, A., 2015b. Powder formulations based on chitosan for nose-to-brain delivery of drugs, JDDST, in press, doi:10.1016/j.jddst.2015.05.002.

Rausch, D.M., Stover, E.S., 2001 Neuroscience research in AIDS. Prog. Neuropsychopharmacol. Biol. Psychiatry 25, 231−257.

Sacchetti, C., Artusi, M., Santi, P., Colombo, P., 2002. Caffeine microparticles for nasal administration obtained by spray drying. Int. J. Pharm. 242, 335–339.

Seki, T., Sato, N., Hasegawa, T., Kawaguchi, T., Juni, K., 1994. Nasal adsorption of zidovudine and its transport to cerebrospinal fluid in rats. Biol. Pharm. Bull. 17,

1135−1137.

Shelley, C.S., Teodoridis, J.M., Park H., Farokhzad O.C., Bottinger, E.P., Arnaout, M.A., 2002. During differentiation of the monocytic cell line U937, Pur alpha mediates induction of the CD11c beta 2 integrin gene promoter. J. Immunol. 168, 3887–3893.

Sinha, V.R., Singla, A.K., Wadhawan, S., Kaushik, R., Kumria, R., Bansal, K., Dhawan, S., 2004. Chitosan microspheres as a potential carrier for drugs. Int. J. Pharm. 274, 1-33.

Sosnik, A., Seremeta, K.P., 2015. Advantages and challenges of the spray-drying technology for the production of pure drug particles and drug-loaded polymeric carriers. Advances in Colloid and Interface Science 223, 40–54.

Strazielle, N., Belin, M.F., Ghersi-Egea, J.F., 2003. Choroid plexus controls brain availability of anti-HIV nucleoside analogues via pharmacologically inhibitable organic anion transporters. AIDS 17, 1473−1485.

Tang, M.W., Kanki, P.J., Shafer, R.W., 2012. A review of the virological efficacy of the 4 World Health Organization-recommended tenofovir-containing regimens for initial HIV therapy. Clin. Infect. Dis. 54, 862-875.

Thorne, R.G., Frey, W.H., 2001. Delivery of neurotropic factors to the central nervous system. Clin. Pharmacokinet. 40, 907−946.

Van den Berg, M. P., Romeijn, S. G., Verhoef, J. C., Merkus, F. W., 2002. Serial cerebrospinal fluid sampling in a rat model to study drug uptake from the nasal cavity. *J. Neurosci. Methods* 2002, *116*, 99–107.

Vyas, T.K., Shahiwala, A., Marathe, S., Misra, A., 2005. Intranasal drug delivery for brain targeting. Curr. Drug Del. 2, 165−175.

Wang, Y., Sawchuk, R.J., 1995. Zidovudine transport in the rabbit during intravenous and intracerebroventricular infusion. J. Pharm. Sci. 7, 871−876.

Wang, H., Wu, L., Reinhard, B.M., 2012. Scavenger receptor mediated endocytosis of silver nanoparticles into J774A.1 macrophages is heterogeneous. ACS Nano. 6(8), 7122-7132

Yagil-Kelmer, E., Kazmier, P., Rahaman, M.N., Bal, B.S., Tessman, R.K., Estes, D.M., 2004. Comparison of the response of primary human blood monocytes and the U937 human monocytic cell line to two different sizes of alumina ceramic particles. J. Orthop. Res. 22, 832–838.

## Figure Captions

**Fig. 1.** Intracellular levels of AZT and its prodrug UDCA-AZT after incubation (30 min) with J774A.1 murine macrophages. The incubation concentrations were 100 μM for AZT and 10 and 100 μM for UDCA-AZT. The graph also reports the intracellular levels of AZT after the incubation of the macrophages with 100 μM UDCA-AZT. The data are reported as the mean±S.D. of three independent experiments. *: $P<0.001$ versus 100 μM AZT.

**Fig. 2.** Size distribution of loaded (CP) and unloaded (CH) chitosan microspheres (up), MIX and chitosan chloride and UDCA-AZT alone, before and after grinding (down). The particle size distribution was graphically expressed as curves obtained by plotting the volume of the particles as a percentage *versus* size (μm), shown on a logarithmic scale

**Fig. 3.** Scanning electron microscopy (SEM) micrographs of the mixture of chitosan chloride and UDCA-AZT (87:13 w/w, magnification of 3,610 times) [A]; ground chitosan chloride (magnification of 3,140 times) [B]; ground UDCA-AZT with magnifications of 512 times [C] and 10,000 times [D]; chitosan chloride before grinding (magnification of 2,740 times) [E]; and UDCA-AZT before grinding (magnification of 505 times) [F].

**Fig. 4.** Scanning electron microscopy (SEM) micrographs of the loaded microparticles (sample CP) with magnifications of 11,250 times [A] and 3,620 times [B].

**Fig. 5.** Water uptake profiles of loaded (CP) and unloaded (CH) microspheres over 60 min in comparison to that of the physical mixture (MIX, chitosan chloride and UDCA−AZT (87:13 w/w). The data are reported as the mean±SD of three independent experiments.

**Fig. 6.** *In vitro* release of UDCA−AZT from CP microparticles based on chitosan chloride. The release profile is compared with the dissolution profile obtained for the parent physical mixture of chitosan chloride and UDCA-AZT (87:13 w/w) (MIX). The data are reported as the mean±SD of three independent experiments.

**Fig. 7.** Elimination profile of AZT after the infusion 0.200 mg of UDCA−AZT into rats. The data are expressed as the mean±SD of four independent experiments. The elimination followed apparent first order kinetics, as confirmed by the semilogarithmic plot reported in the inset ($n = 9$, $r = 0.990$, $P < 0.0001$). The half-life of AZT was calculated to be 60.4±3.8 min.

**Fig. 8.** UDCA−AZT concentrations (μg/mL) detected in the CSF after the nasal administration of dry powders constituted by loaded CP microparticles and its parent mixture (MIX) of chitosan chloride and UDCA-AZT. Each dose contained 200 μg of the prodrug. The inset reports the semilogarithmic plot of the UDCA-AZT concentrations (μM) in the CSF after the nasal administration of the CP sample. The elimination of UDCA-AZT from the CSF followed apparent first order kinetics, as confirmed by the linear regression of the points ranging from 60 to 180 min ($n = 4$, $r = 0.988$, $p < 0.05$). The data are expressed as the mean±SD of four independent experiments.

**Fig. 9.** A comparison among the AUC values obtained in the CSF of rats after the nasal administration of 200 μg of UDCA-AZT using different formulations (i.e., loaded solid lipid microparticles (SLMs), their water dispersion in the presence of chitosan (SLMs + Ch), the physical mixture of chitosan and prodrug (MIX) and the loaded microparticles based on chitosan chloride (CP)). The data pertaining to SLMs and the SLM + Ch formulations were reported previously (Dalpiaz et al., 2014). The data are expressed as the mean±SD of four independent experiments.

1

**Table 1.**

Volume-surface diameters ($d_{vs}$, μm) of unloaded (CH) and loaded (CP) microparticles together with $d_{vs}$ values of the parent mixture (MIX) of chitosan chloride and UDA-AZT and its single components before and after grinding by agate mortar and pestle. Data are reported as the mean ± SD of three independent experiments.

| Sample | $d_{vs}$ (μm) |
|---|---|
| CP | 3.59 ± 0.14 |
| CH | 2.32 ± 0.11 |
| MIX | 6.11 ± 0.02 |
| Grinded Chitosan HCl | 12.67 ± 0.82 |
| Grinded UDCA-AZT | 5.12 ± 0.02 |
| Chitosan chloride before grinding | 19.98 ±0.06 |
| UDCA-AZT before grinding | 23.33 ± 0.06 |

**Figure 1**

Click here to download high resolution image

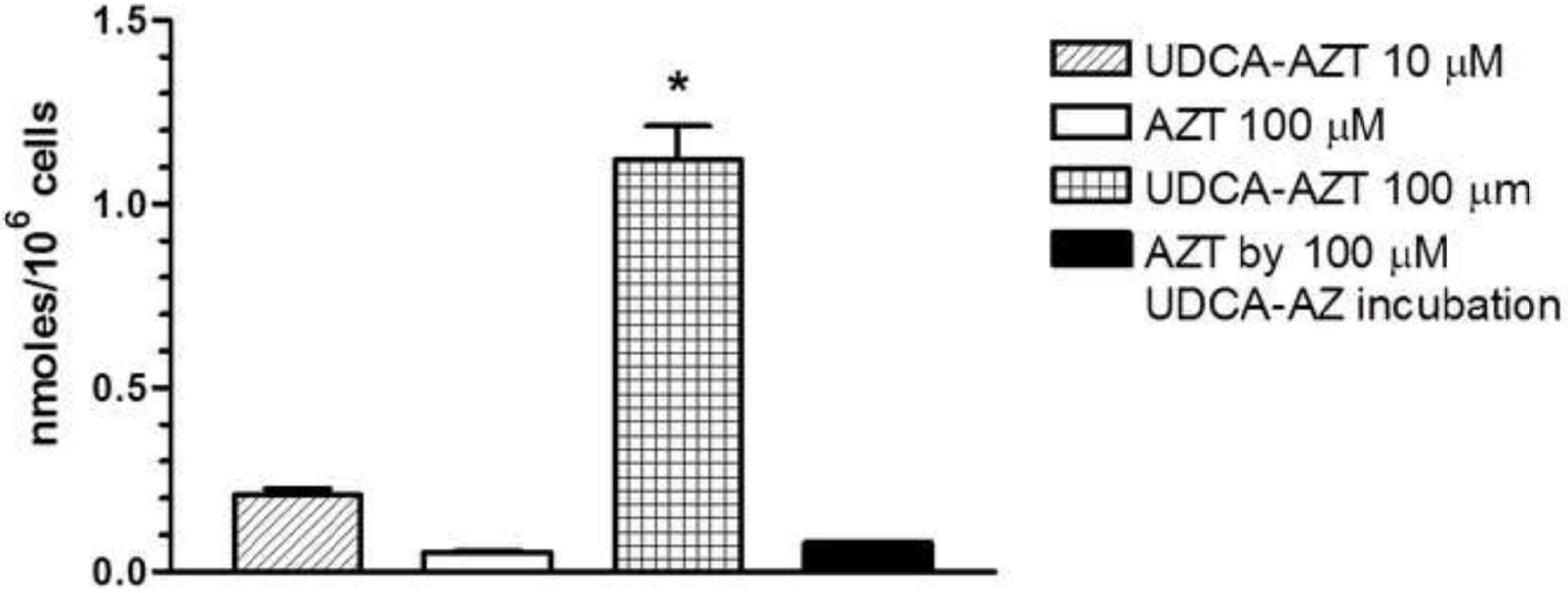

**Figure 2**

**Click here to download high resolution image**

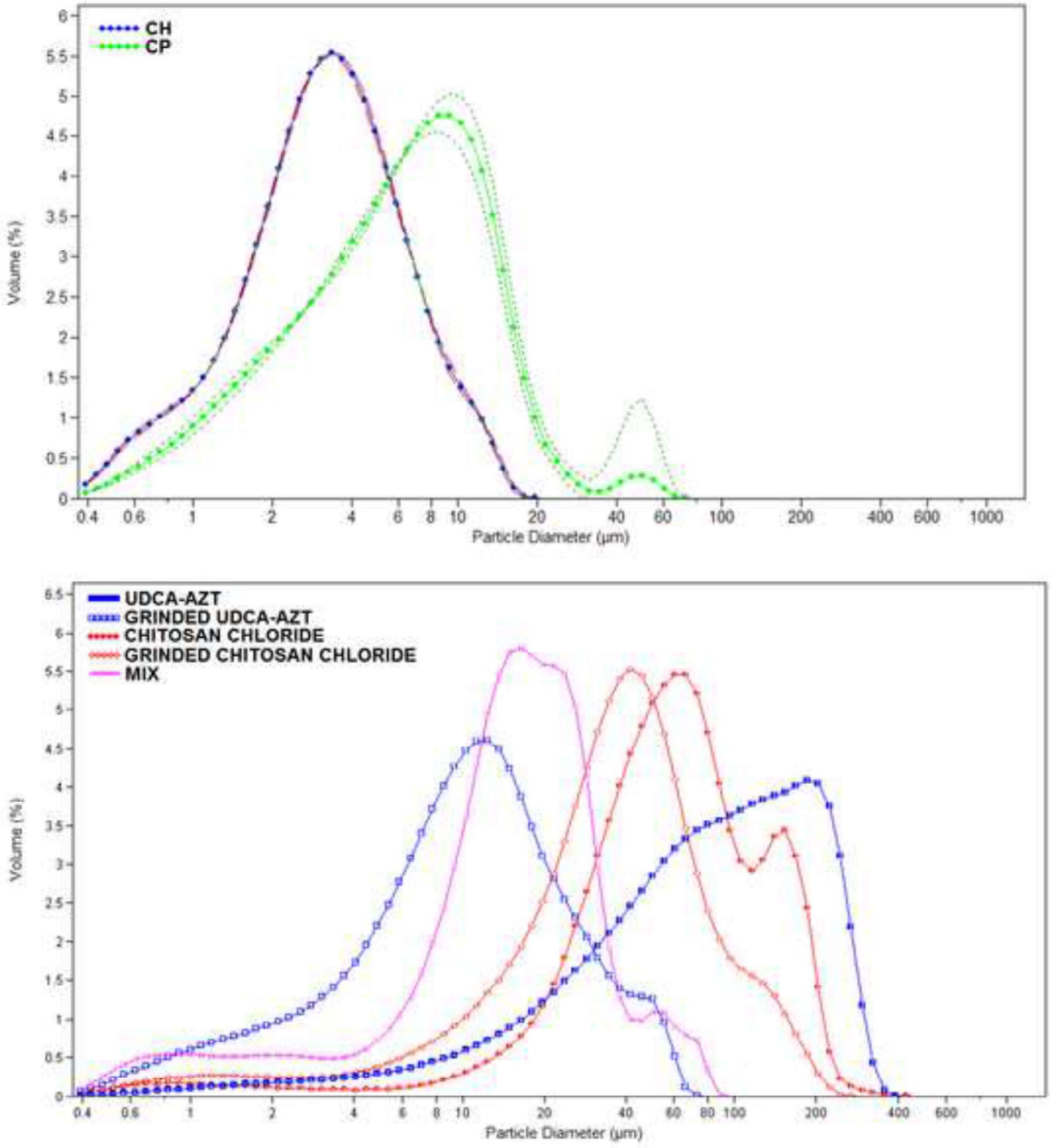

**Figure 3**

**Click here to download high resolution image**

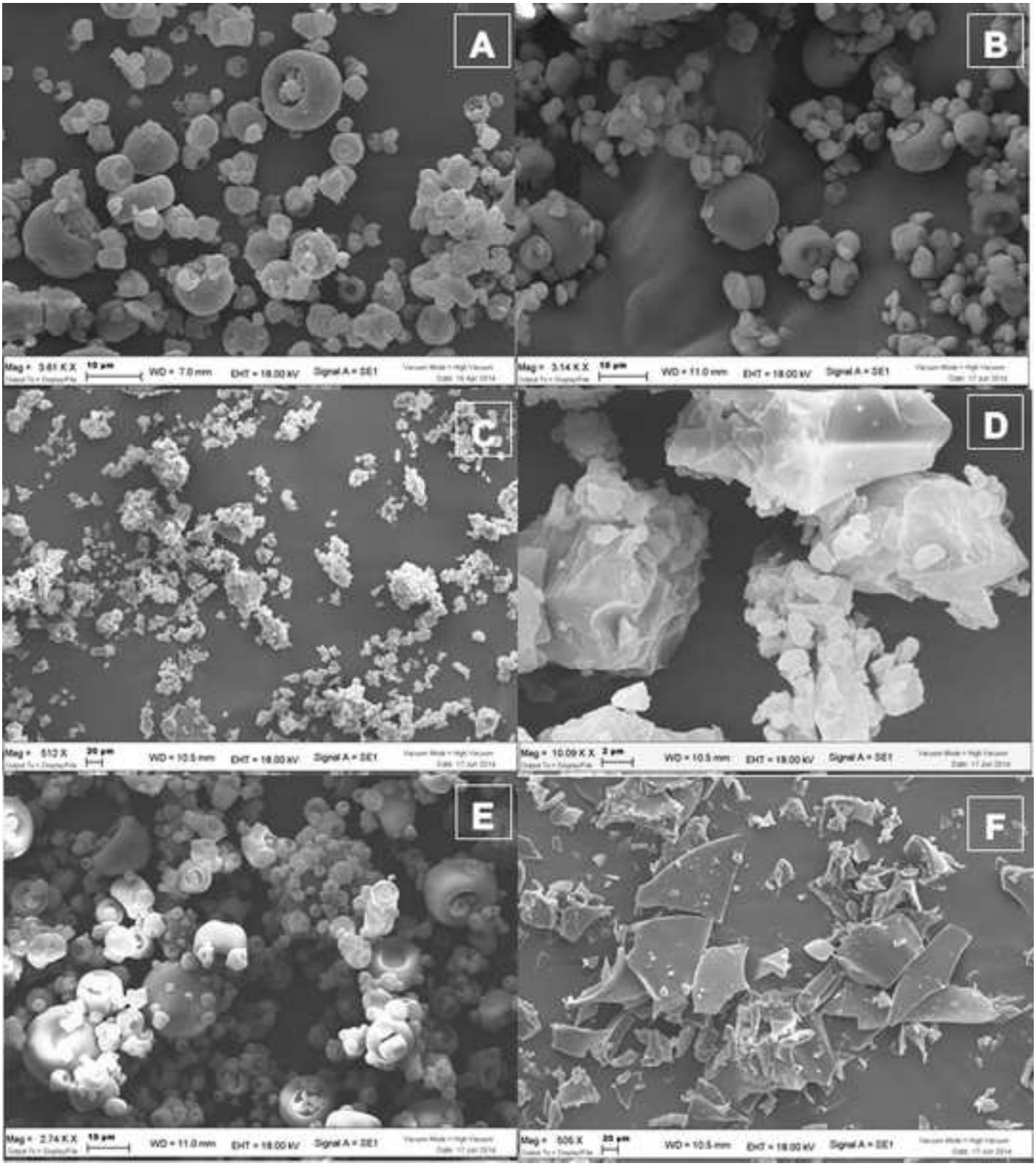

**Figure 4**

Click here to download high resolution image

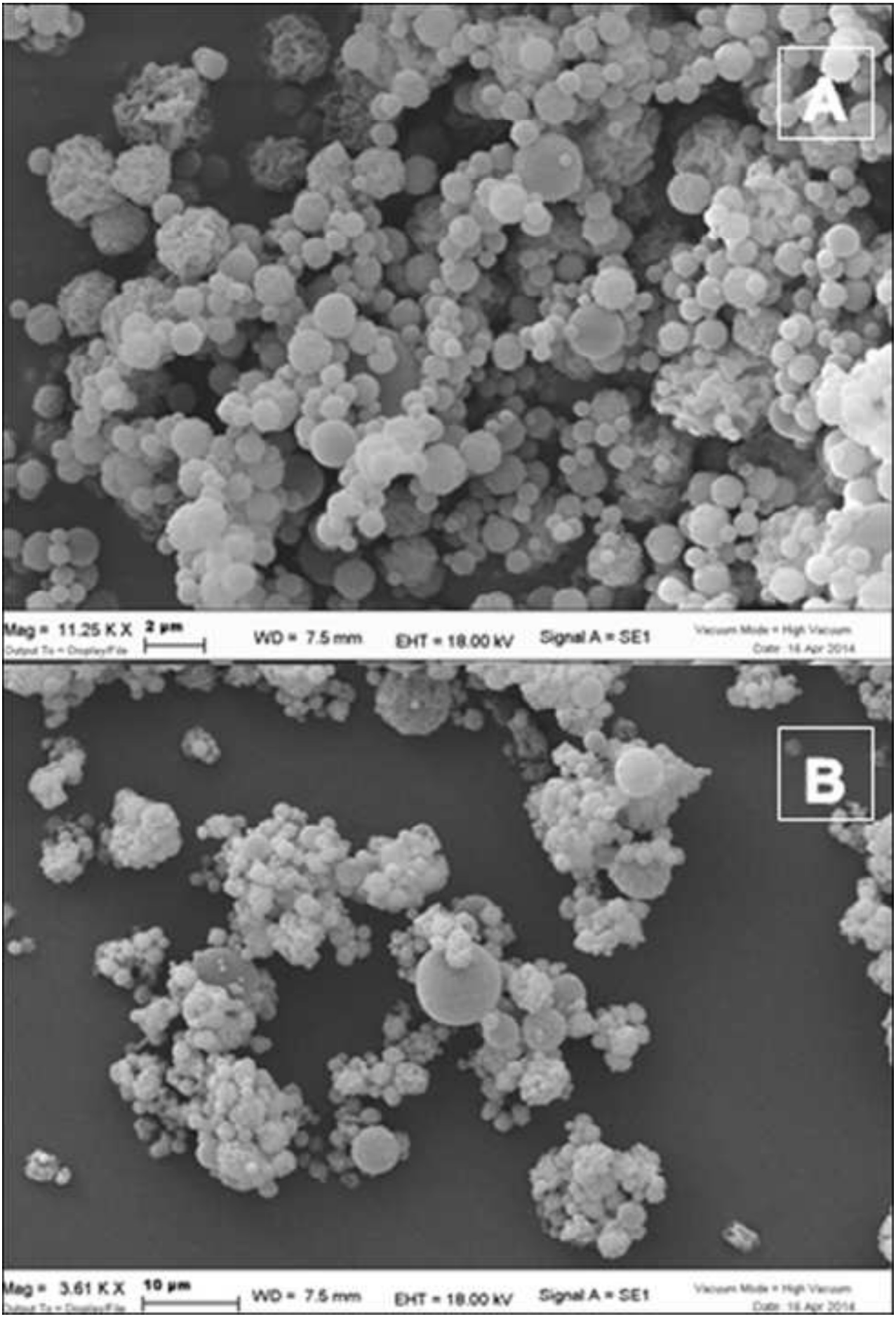

Figure 5
Click here to download high resolution image

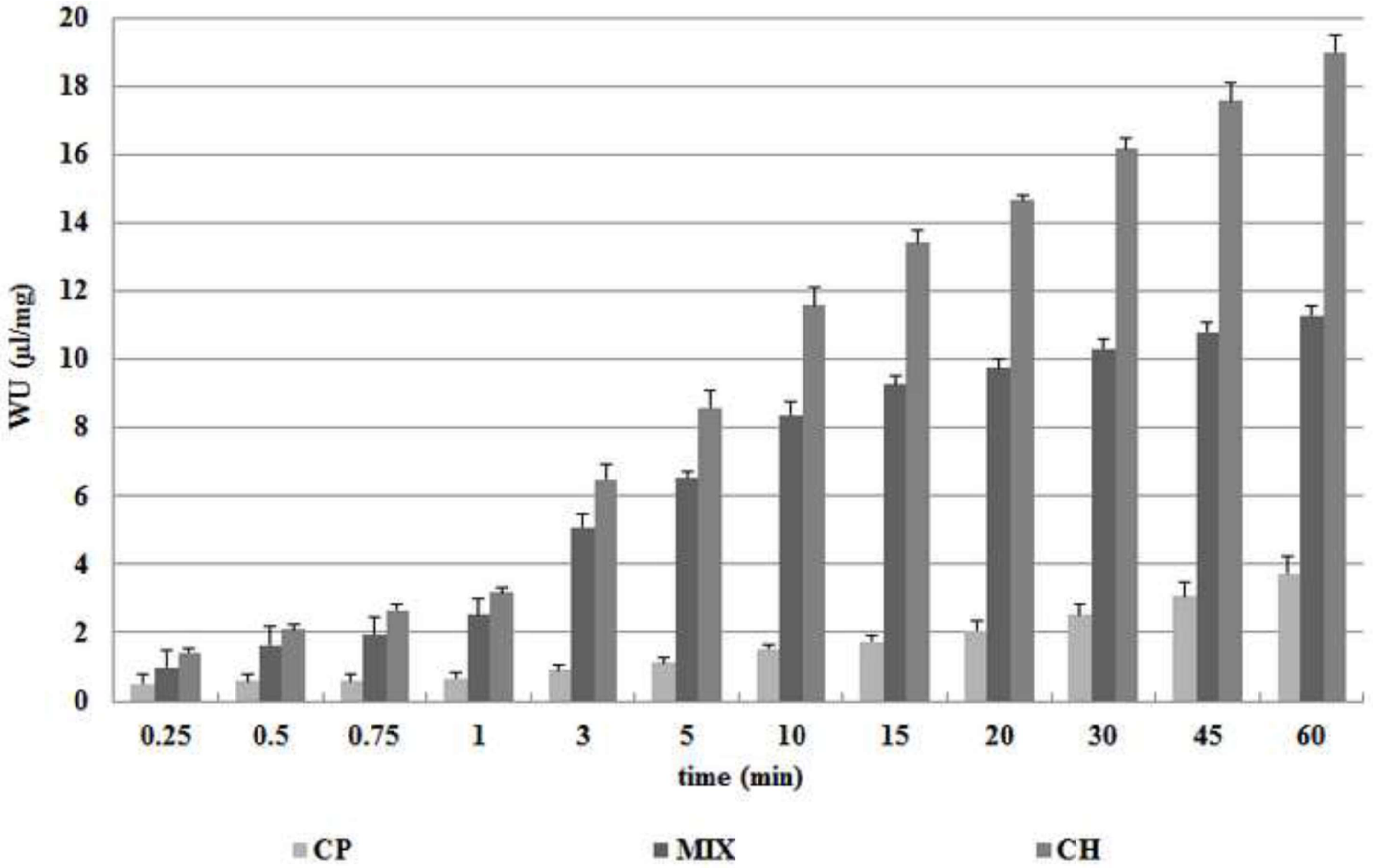

Figure 6
Click here to download high resolution image

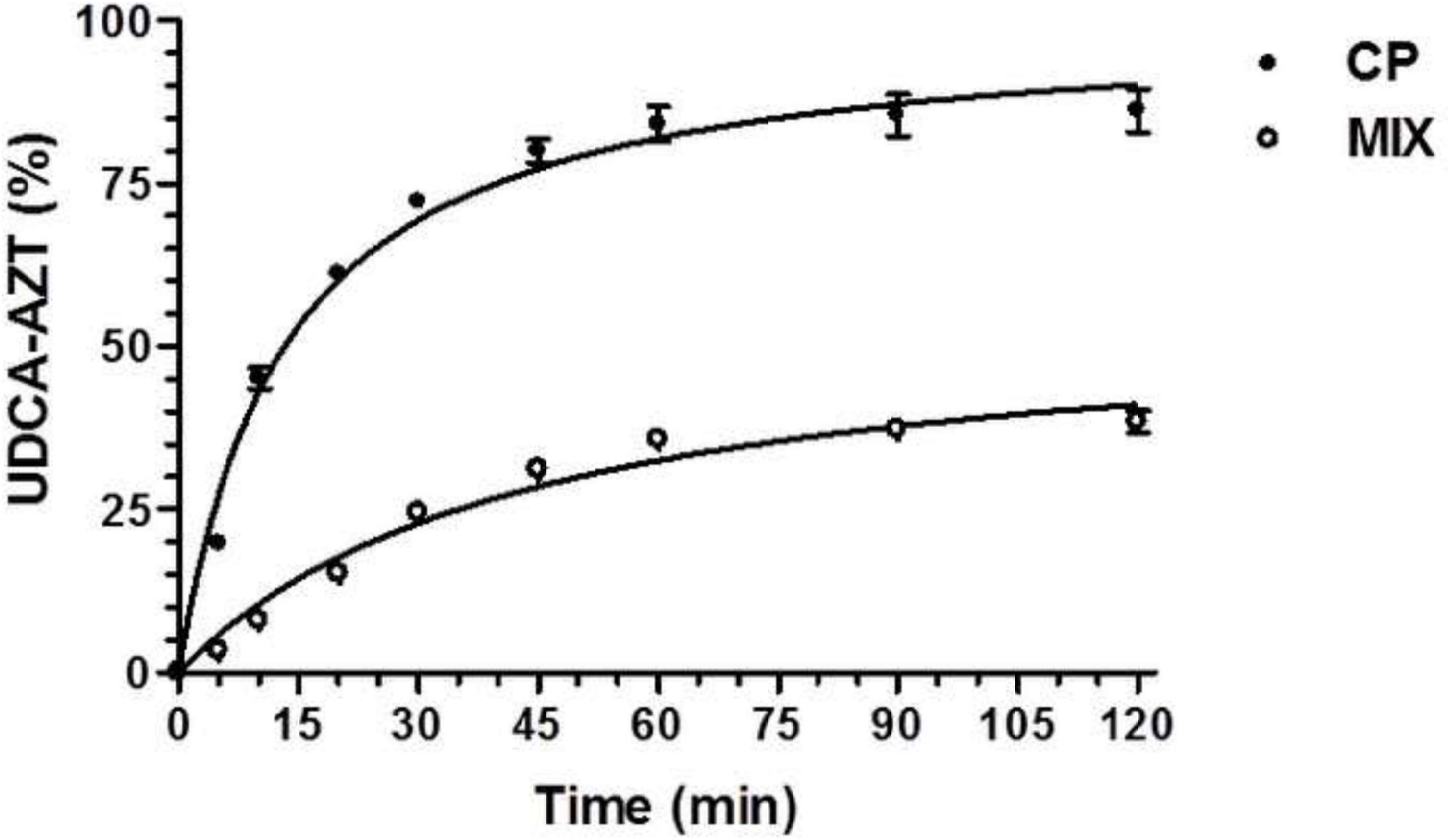

Figure 7

Click here to download high resolution image

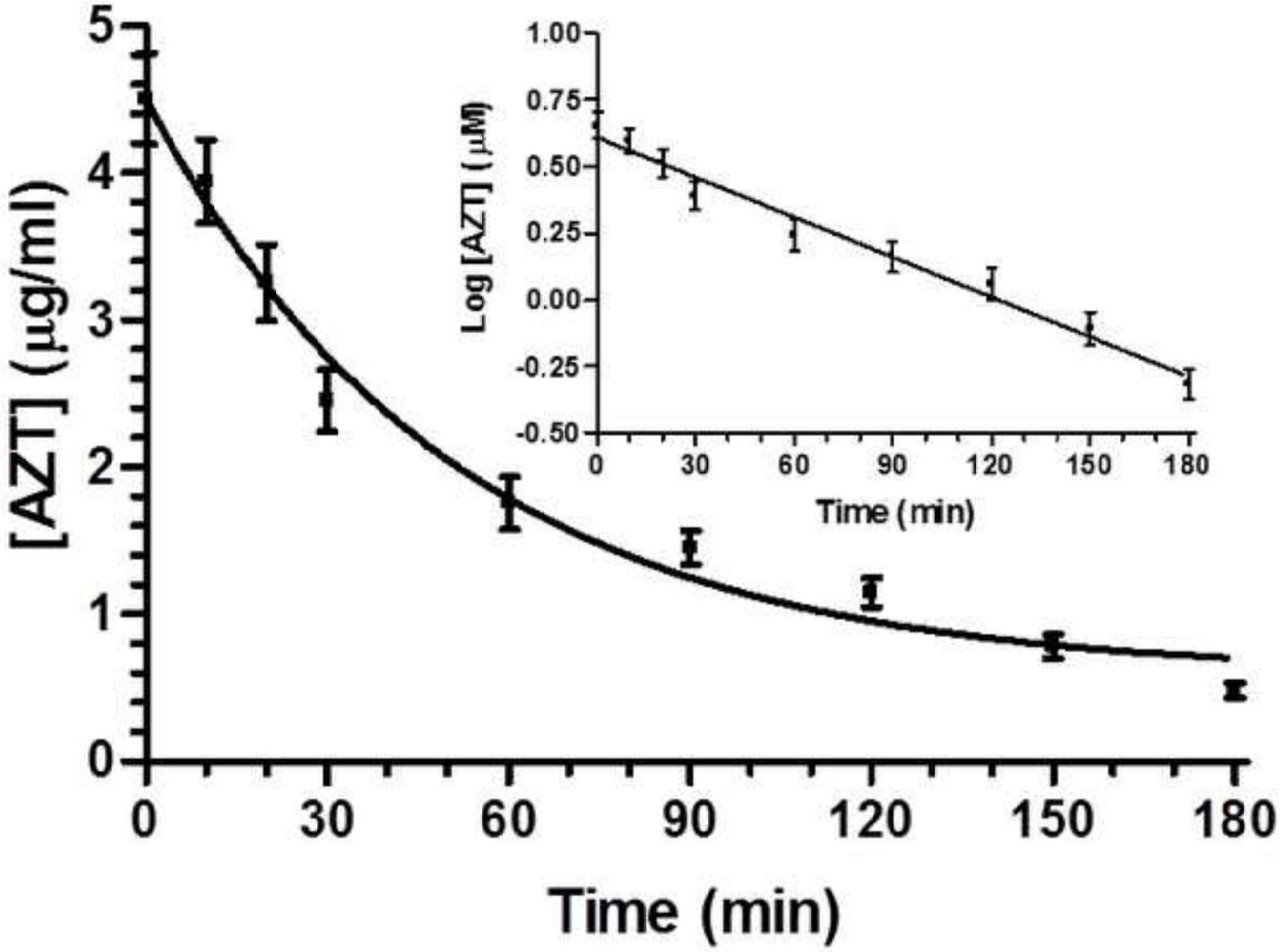

Figure 8

Click here to download high resolution image

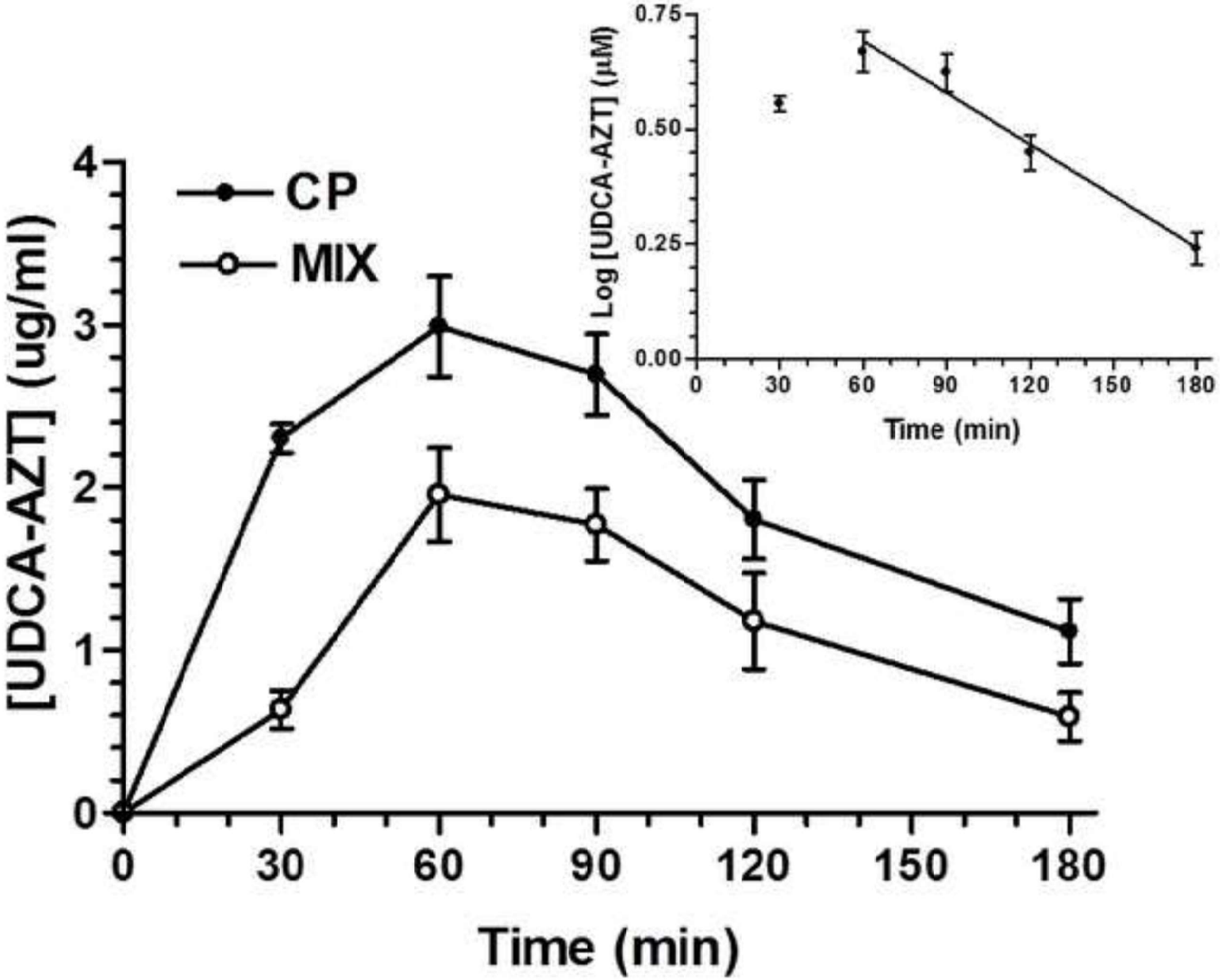

Figure 9
Click here to download high resolution image

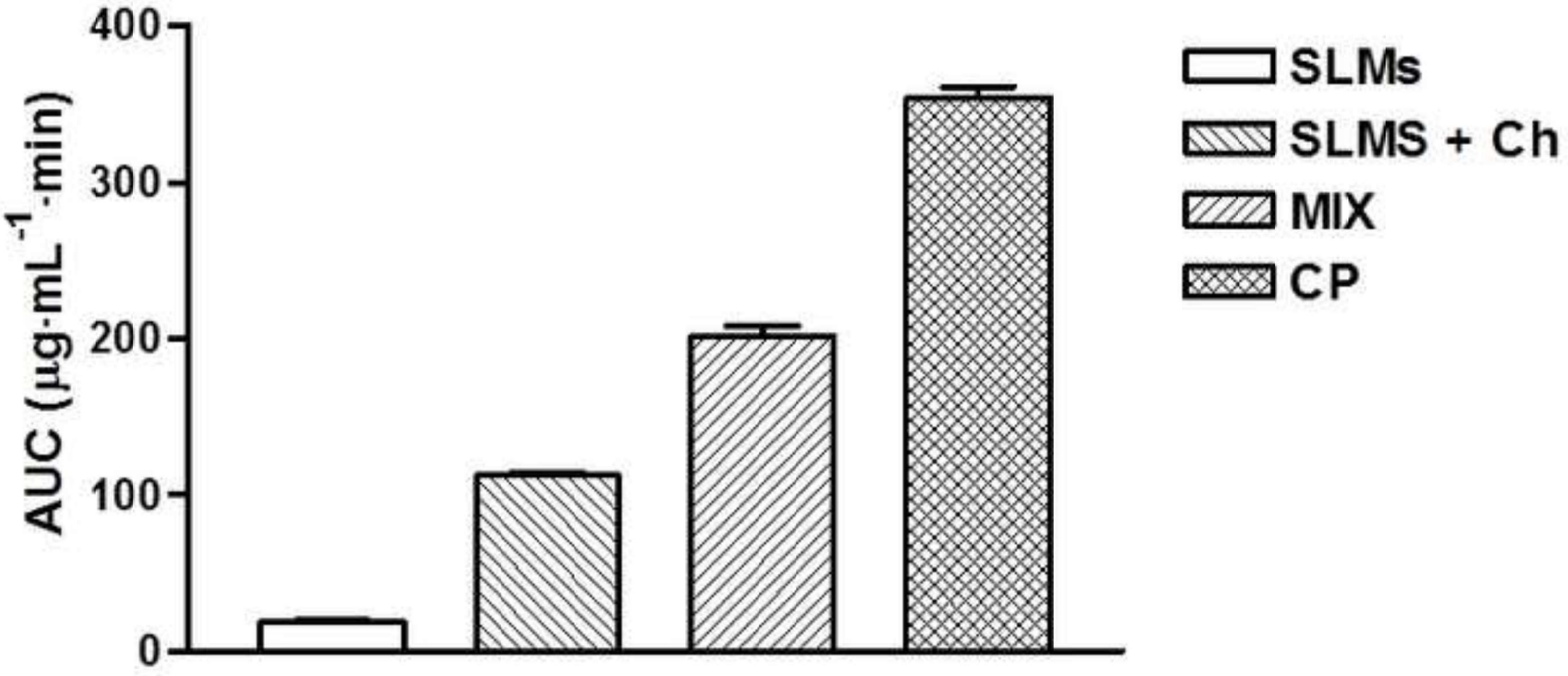

**Graphical abstract**

Click here to download high resolution image